Bidirectional Optogenetic Modulations of Peripheral Sensory Nerve Activity: Induction vs. Suppression through Channelrhodopsin and Halorhodopsin

Akito Kosugi[1], Ken-ichi Inoue[2], Masahiko Takada[2], and Kazuhiko Seki[1*]

[1]Department of Neurophysiology, National Institute of Neuroscience, National Center of Neurology and Psychiatry, Kodaira, Tokyo 187-8502, Japan

[2]Systems Neuroscience Section, Department of Neuroscience, Primate Research Institute, and Center for the Evolutionary Origins of Human Behavior, Kyoto University, Inuyama, Aichi, 484-8506, Japan

***Corresponding author:** Kazuhiko Seki, Ph.D.

Department of Neurophysiology, National Institute of Neuroscience, National Center of Neurology and Psychiatry, Kodaira, Tokyo 187-8502, Japan

Phone: +81-42-346-1724

E-mail: seki@ncnp.go.jp

Summary

In this study, we investigated the potential of optogenetics for modulating activity of peripheral sensory nerves, particularly tactile and proprioceptive afferents, which are vital for movement control. Using adeno-associated virus serotype 9 vector, we selectively transduced channelrhodopsin (ChR2) and halorhodopsin (eNpHR3.0) into large-diameter sciatic nerve afferents of rats. Diverging from conventional dorsal root ganglion (DRG) approaches, we applied optical stimulation at the distal portion of the afferent nerve. The intensity of optical stimulation varied to modulate the extent of induction and suppression of afferent activity. Then, the effect of optical stimulation was determined by the activity recorded in the dorsal root of the same afferents. Our findings show successful induction and suppression of activity in large-diameter afferents via optical stimulation. By increasing the intensity of blue (for ChR2) and yellow (for eNpHR3.0) light stimulation, the activity of fast-conducting afferent fibers was preferentially evoked or inhibited in an intensity-dependent manner. These data indicate that the activity of large-diameter afferents can systematically be regulated by optogenetics. The present innovative methodology for manipulating specific sensory modalities at the nerve level offers a targeted and accessible alternative to DRG stimulation, expanding the therapeutic scope of optogenetics for treating sensory disorders.

Keywords: adeno-associated virus, peripheral nerve, dorsal root ganglion neuron, touch,

proprioception

Introduction

Peripheral sensory nerve activity is integral in conveying sensory experiences to the central nervous system (CNS). Dysregulation of the peripheral sensory nerves, manifesting hyper- or hypoactivation, is a hallmark of various sensory disorders (1, 2). Conventional treatments for regulating peripheral nerve activity, such as pharmacological and electrical interventions (3−6), often lack specificity and may introduce adverse effects (4, 7, 8). The advent of optogenetics – a technique that manipulates neural activity with light-sensitive proteins – offers an alternative solution with unprecedented temporal and spatial precision that has already been established in the CNS (9−15).

In the present study, we attempted the extension of this optogenetic technique to peripheral sensory nerves, specifically targeting large-diameter afferents associated with tactile and proprioceptive sensations. The dorsal root ganglion (DRG) is the standard site for neural modulation (16−19), but is encumbered by its anatomical complexity and procedural risks (20, 21). By contrast, peripheral nerves are more accessible targets with reduced complexity, as evidenced by successful optogenetic manipulation of motor neuron axons (22−25). The heterogeneity of peripheral sensory nerves, comprising afferents of varying modalities and diameters (26−29), introduces specific challenges for optogenetic application. Our previous work demonstrated the efficacy of adeno-associated virus serotype 9 (AAV9) vector for gene transduction into DRG neurons linked to fast-conducting primary afferent

58 fibers (19, 30). In this study, we used the AAV9 vector to target selectively large-diameter
59 sensory fibers in the sciatic nerve of rats transduced with a light-activated ion channel,
60 channelrhodopsin (ChR2), and a light-driven chloride pump, halorhodopsin (eNpHR3.0). We
61 found that optical stimulation of the sciatic nerve evoked or suppressed action potentials in its
62 afferent fibers, with the magnitude of effect directly proportional to the light intensity. This
63 suggests the feasibility of optogenetic approaches to fine regulation of sensory signals
64 transmitted through peripheral nerve fibers.
65

Results

Transduction of ChR2 and eNpHR3.0 Using AAV9 Vector

We successfully transduced ChR2 (n = 7) or eNpHR3.0 (n = 10) into DRG neurons by intra-nerve injection of AAV9 vector (Fig. 1A and B). Using an acute experimental setup, we evaluated the effect of optical stimuli on the distal portion of the sciatic nerve (Fig. 1C and E).

Optogenetic Induction and Suppression of Sensory Afferent Activity

In rats transduced with ChR2, the effect of blue light was examined by recording the conducting afferent volleys at the dorsal root (Fig. 1C). For rats transduced with eNpHR3.0, the nerve was pre-activated by electrical stimulation, and the effect of yellow light applied proximally to the stimulation site was then assessed at the dorsal root (Fig. 1E). Representative results are shown in Figure 1D and F. Specifically, in the ChR2-transduced rats, 470-nm light produced long-lasting volleys in the dorsal root, while 593-nm light had no modulatory effect (Fig. 1D). In the eNpHR3.0-transduced rats, the volley size evoked by electrical stimulation (Fig. 1F, gray line) was significantly diminished by optical stimulation at 593 nm (Fig. 1F, black line, and Fig. S1B). We found comparable induction or significant suppression of action potentials in all ChR2- (n = 7) and eNpHR3.0-transduced rats (n = 10). Since this is the first study to inhibit action potential conduction at the peripheral nerve level,

we further characterized the optogenetic suppression and confirmed a stable and reversible manner for inhibiting action potential conduction (Fig. S1). These findings demonstrated that light application could effectively evoke action potentials in sensory fibers of the ChR2-transduced rats and suppress sensory fiber activity in the eNpHR3.0-transduced rats.

Modulations of Sensory Afferent Activity Dependent on Optical Stimulation Intensity

Next, we examined the impact of varying optical stimulation intensity on sensory afferent activity. In the ChR2-transduced rats, increasing the intensity of blue light from 20.5 to 51.6 mW resulted in a gradual increase in the amplitude of the recruited volley (Fig. 2A and B; significant main effect of light power analyzed by Friedman's test, $\chi^2_{(6,60)} = 63.9$, $p < 0.0001$). In eNpHR3.0-transduced rats, on the other hand, increasing the power of yellow light (≥ 8.7 mW) gradually decreased the amplitude of the electrically evoked volley (Fig. 2D and E; significant main effect of light power analyzed by Friedman's test, $\chi^2_{(9,81)} = 73.8$, $p < 0.0001$). These observations confirmed that optical stimulation could regulate the amplitude of recruited volleys by tuning the stimulation intensity. In addition, increasing the light power resulted in a shorter onset latency of the recruited volley in the ChR2-transduced rats (Fig. 2C) and a longer onset latency of the electrically evoked volley in the eNpHR3.0-transduced rats (Fig. 2F, latency suppression). The overall findings indicate that sensory afferent nerve activity can be finely controlled by adjusting optical stimulation parameters.

104

105 **Selective Modulation of Large-diameter Afferent Activity**

106 Next, we examined the afferent selectivity of optogenetic modulation, given the tropism of
107 AAV9 vector for fast-conducting, large-diameter afferents (19, 30). In the ChR2-transduced
108 rats, the lower power of optical stimulation exclusively recruited early-onset volleys, while
109 its higher power additionally recruited late-onset volleys as well (Fig. 3A). Specifically,
110 early-onset volleys were not observed at 11.4 mW irradiation, but became apparent at around
111 20.5 mW irradiation (Fig. 3B). By increasing the light power, late-onset volleys were first
112 observed at around 64.7 mW (Fig. 3B). This outcome aligned with the expected large-
113 diameter selectivity of AAV9 vector. We further compared the maximal amplitude between
114 the early-onset (1.5–4 ms after stimulus onset; Fig.3A, red shading) and the late-onset (5–10
115 ms after stimulus onset; Fig.3A, blue shading) volleys. The earlier range corresponded with a
116 conduction velocity of 15–45 m/s, which well fitted within the expected range for fast-
117 conducting, large-diameter Aα/β fibers (> 14 m/s) (31). The results showed that the amplitude
118 was larger in volleys with shorter latencies (Fig. 3C; Wilcoxon signed-rank test, $p = 0.016$).
119 Therefore, we concluded that large-diameter afferents, potentially Aα/β fibers, were
120 preferential targets for optogenetic induction and modulation in the ChR2-transduced rats.

121 For the eNpHR3.0-transduced rats, we also confirmed preferential regulation of
122 large-diameter afferents. We increased the intensity of electrical stimulation to determine how

optical stimulation with the same parameters suppressed the size of electrically evoked volleys. We found a marked effect on volleys evoked by a stimulus current just above the recruitment threshold (1T in Fig. 3D). Notably, these lowest-threshold volleys were eliminated (100% amplitude inhibition) by optical stimulation in five of the 10 animals. By contrast, the optical stimulation did not eliminate the volley evoked at 2T, and the suppressive effect was less marked at 5T. We quantified the relationship between the suppressive effect and the electrical current in this animal (Fig. 3E). As reported earlier (32, 33), without optical stimulation, the volley size first increased rapidly and then slowly as a function of electrical current. With optical stimulation, however, this relationship changed from a non-linear to a more linear manner, and the size of the volley linearly increased as a function of current. This suggests the possibility that the suppressive effect may be afferent selective. For example, optogenetic suppression was more effective in the volley evoked at 2T (57%) than 5T (6%; ratio of gray line to black line in Fig. 3E). We calculated the efficacy of inhibition of the volley amplitude in all animals (Fig. 3F) and found that it was indeed larger for volleys evoked by a lower stimulus current. Maximal efficacy was obtained at around 1T and then decreased quickly, though it was still obvious until at 2T. The inhibitory effect was not statistically significant (Fig. 3F; one-tailed Wilcoxon signed-rank test, p = 0.063 without Holm–Bonferroni correction) despite that the stimulation intensity was increased to five times as much as the threshold level. We also found a comparable change in

142 the onset latency of volleys. Indeed, the efficacy to generate a late-onset latency was
143 decreased in volleys evoked by a higher stimulus current (Fig. 3G and H). These findings
144 showed that optogenetic suppression had a greater effect on volleys evoked by lower-
145 intensity electrical stimulation, suggesting preferential suppression of large-diameter afferent
146 fibers. The overall results indicate that large-diameter sensory afferent activity can selectively
147 be evoked and suppressed by optogenetics.
148

149 **Correlation Between Efficacy of Gene Expression and Extent of Optogenetic**
150 **Modulation**

151 We examined the relationship between the gene expression levels and the optogenetic
152 modulation effects in both the ChR2- and the eNpHR3.0-transduced rats (Fig. 4). An example
153 in Figure 4A shows recruited volleys and yellow fluorescent protein (YFP) expression in
154 DRG neurons of two ChR2-transduced rats with varying expression levels. One animal
155 exhibited larger efficacy in optical stimulation and stronger YFP signal intensity. We found a
156 significant correlation coefficient between the maximal magnitude of recruited volleys and
157 the YFP signal intensity (Fig. 4B; $r = 0.99$, $p < 0.0001$). A similar comparison was done in the
158 eNpHR3.0-transduced rats (Fig. 4C). Again, a significant correlation coefficient was found
159 between the amplitude inhibition percentage and the YFP signal intensity (Fig. 4D; $r = 0.88$,
160 $p = 0.001$). It should be noted here that these significant correlations were maintained when

161 an animal with notably high YFP expression was excluded (ChR2: $r = 0.82$, $p = 0.047$;
162 eNpHR3.0: $r = 0.68$, $p = 0.043$). The results indicate the importance of consistent expression
163 efficacy across animals for reproducible optogenetic modulation of sensory afferent activity.
164 Overall, our findings lead to similar conclusions in both of the ChR2- and the
165 eNpHR3.0-transduced rats regarding the stimulation intensity-dependent modulation of large-
166 diameter sensory afferent fibers and the correlation between the optogenetic effects and the
167 gene expression efficacy. However, a notable difference was also observed between the two
168 rat models, as described below.
169
170 **DRG vs. Nerve: Comparative Analysis of Light Irradiation Sites**
171 Building on previous studies that reported the optogenetic modulation of sensory afferent
172 activity through light irradiation toward DRG neurons (7, 16−19), we next aimed to compare
173 the efficacy of modulation between optical stimulation of DRG neurons and peripheral nerve
174 fibers.
175 In the ChR2-transduced rats, we found that nerve-evoked volleys exhibited smaller
176 amplitudes compared with DRG-evoked volleys (Fig. 5A–C). Since we applied the same
177 intensity of optical stimulation in both conditions, this indicates that induction of sensory
178 afferent activity by nerve irradiation is less effective than by classical DRG stimulation (Fig.
179 5C; Wilcoxon signed-rank test, $p = 0.016$).

Contrastingly, in the eNpHR3.0-transduced rats, suppression of afferent fiber activity through nerve irradiation displayed the superior efficacy to DRG irradiation. This was demonstrated by more pronounced suppression of sensory afferent activity upon optical stimulation of the nerve compared with the DRG stimulation (Fig. 5D and E; Wilcoxon signed-rank test, $p = 0.031$).

These findings collectively suggest that while optical stimulation of sensory afferent fibers and DRG are capable of both inducing and suppressing their activity (as shown in Figs. 1–4), its effectiveness varies depending on the irradiation site. Specifically, in the eNpHR3.0-transduced rats, nerve irradiation exhibited more prominent suppression of activity compared with the classical DRG irradiation approach. Conversely, in the ChR2-transduced rats, the nerve application proved to be less effective in inducing sensory afferent activity. Such an efficacy difference highlights the significance of selecting the appropriate irradiation site to achieve the desired outcome in optogenetic modulation of sensory afferents. Notably, for induction of sensory afferent activity, the DRG may be a preferable choice, despite the increased complexity and surgical challenges associated with access thereto. This consideration is critical when weighing the trade-off between the efficacy and the procedural complexity in optogenetic manipulation of sensory pathways.

Discussion

199 There are three points of novelty in the present study. First, we have succeeded in inducing
200 and suppressing peripheral sensory nerve activity by optical stimulation. Second, the activity
201 of fast-conducting, large-diameter afferent fibers was preferentially evoked or suppressed in a
202 stimulation intensity-dependent manner. Third, the efficacy of optical stimulation varied
203 depending on the irradiation site. In particular, the peripheral nerve was the preferred target
204 for optogenetic suppression.
205

206 **Optogenetic Control of Peripheral Nerve Activity**

207 In our study, we have found that optical stimulation can recruit primary afferent activity, with
208 their amplitude and onset latency modulated in an intensity-dependent manner. A previous
209 study reported that optical stimulation activated opsins expressed in axons at the node of
210 Ranvier and generated action potentials (34). When the estimated conduction velocity of
211 optically evoked volleys was investigated in the present study, it was consistently within the
212 range of fast-conducting, large-diameter Aα/β fibers (> 14 m/s) (31). This implies the
213 induction of Aα/β fiber activity by optical stimulation. In addition, our data confirmed
214 recruitment of high-threshold late component volleys upon optical stimulation at high
215 intensity with longer light-pulse durations, suggesting an off-target effect of optical
216 stimulation (19). Nevertheless, the amplitude for late component volleys was usually smaller
217 than for early component volleys (Fig. 3B and C). Thus, we can conclude that the optical

218 stimulation in this study preferentially induces the activity of Aα/β fibers.

219 We also effectively demonstrated optogenetic suppression of axonal action
220 potentials which were beforehand activated at the time of stimulation. When the action
221 potentials were generated by electrical stimulation near the threshold current, we observed
222 almost complete elimination of electrically evoked volleys. Electrical nerve stimulation is
223 known to recruit action potentials in accordance with axonal diameter, as axons with larger
224 diameters offer lower electrical resistance, making them more susceptible to depolarization in
225 response to smaller input signals (35, 36). The earliest component of the recorded volleys,
226 known as the "Aα" wave, reflects action potentials generated by group I muscle afferent
227 fibers, which possess the largest axonal diameter among various categories of primary
228 afferents (33, 37−39). Consequently, the complete elimination of volleys by optogenetic
229 suppression in this study (Fig. 3D) indicates the superior effectiveness of optical stimulation
230 in suppressing the activity of group I afferents. We also found the efficient optogenetic
231 suppression of axonal action potentials primarily evoked by electrical stimulation at
232 intensities twice as much as their recruitment threshold or below. It is well established that at
233 such stimulation intensities, activities of both group I and II afferents are introduced, whereas
234 finer afferents (like those of group III) are not activated (32). Therefore, we suggest that
235 optogenetic manipulation in this study indeed inhibits the activity of large-diameter primary
236 afferents, such as group I and II fibers.

237 Until recently, optogenetic suppression of primary afferent activity has exclusively
238 been demonstrated by targeting small-diameter DRG neurons that are responsible for
239 transmitting nociceptive signals (7, 17, 18, 40–42), with limited attention given to large-
240 diameter neurons. In an effort to fill this gap, we previously attempted to transduce genes by
241 intra-nerve injection of AAV9 vector (19, 30), known for its affinity toward medium-to-large-
242 sized DRG neurons that are involved in conveying mechanoreceptive and proprioceptive
243 signals (43). Here, we have further extended our approach using the AAV9 vector to achieve
244 not only excitation (19), but also inhibition of large-diameter primary afferents including
245 group I and II fibers.
246
247 **DRG vs. Nerve**
248 Theoretically, there are four possible locations for light irradiation to activate opsins
249 expressed in the peripheral sensory system: peripheral tissue, spinal cord, DRG, and
250 peripheral nerve (5, 44). Among these, targeting the peripheral tissue has limitations. Light
251 penetration is restricted to skin tissue when it is irradiated from the body surface (24), thereby
252 confining the modulatory effect to skin receptors. The impact on deep primary afferent
253 terminals, such as muscle spindles and Golgi tendon organs, is either impossible or
254 incomplete. Similarly, targeting the spinal cord (from its surface) is inefficient due to the
255 highly myelinated dorsal white matter which makes the light scattered (45, 46). Light

256 intensity is likely to be significantly diminished before reaching the intermediate layer of the
257 spinal cord where group I fibers terminate. In the present study, we targeted the remaining
258 two candidates, DRG and peripheral nerve, and revealed that targeting the DRG yielded a
259 superior efficacy for optogenetic induction of large-diameter primary sensory afferents,
260 whereas targeting the peripheral nerve had the advantage of their suppression.

261 These observed differences in the effectiveness of optical stimulation between the
262 DRG and the peripheral nerve suggest the involvement of distinct mechanisms. In the
263 peripheral nerve, light irradiation activates opsins expressed in axons and changes the intra-
264 axonal potential (34). By contrast, irradiation toward the DRG leads to activation of opsins
265 expressed not only in axons, but also in somata. It was our expectation that the effect of light
266 irradiation might be amplified by addition of the somal effect. This is because DRG neurons
267 have active ion channels in their somata and can generate action potentials (47, 48), although
268 these action potentials are generally believed to be rare. Also, hyperpolarization of the somata
269 can influence the membrane potential at the T-junction of DRG, where axonal bifurcation
270 occurs within DRG. Hyperpolarization at the T-junction may interfere with action potential
271 propagation due to the possible impedance mismatch (49, 50). It seemed surprising that we
272 obtained the expected result on optogenetic induction but the opposite result on optogenetic
273 suppression, indicating a lower efficacy of DRG irradiation. Here, we propose two potential
274 explanations for this outcome. First, the anticipated contribution of T-junction

275 hyperpolarization may have been less influential than axonal hyperpolarization. Second, the
276 effect of axonal hyperpolarization due to DRG irradiation may have been minor compared to
277 nerve irradiation, stemming from structural differences between the two. Specifically, somata
278 and satellite cells are located predominantly in the dorsomedial region of DRG, while passing
279 fibers are more evenly distributed throughout the rest of the ganglion (51). Such a location of
280 somata and satellite cells may result in scattering of the light when irradiated from the DRG
281 surface, diminishing its intensity by the time it reaches the axons.

282 The superior efficiency of optical stimulation targeting the nerve, compared with
283 targeting the DRG, is desirable for *in vivo* application of this technique. In the past, various
284 chronic optical stimulation tools have been developed, such as nerve cuffs with LED or
285 optical fibers (52−54), LED directly placed on the peripheral nerve (42), and even
286 transdermal light irradiation to the peripheral nerve (24, 55). Conversely, methods for chronic
287 optical DRG stimulation are limited *in vivo* (44) and are highly invasive, posing a risk of
288 damaging DRG neurons during exposure at the stimulation site (20). Optical stimulation,
289 especially for optogenetic suppression, at the peripheral nerve level opens new experimental
290 possibilities of studying the involvement of sensory afferents in a variety of motor behaviors.
291

292 **Clinical implications**

293 Damage to the CNS in the case of stroke and neurodegenerative diseases, including spinal
294 muscular atrophy (SMA), lead to maladaptive changes in the periphery. In stroke, one
295 common complication is spasticity, which results from hyperexcitability of the spinal reflex
296 (56, 57). While it is assumed that reducing proprioceptive input to the spinal cord could help
297 prevent the onset of spasticity, there has been no clinical treatment to date that offers selective
298 and reversible manipulation of proprioceptive afferents. Similarly, SMA is characterized by
299 motor neuron death and muscle atrophy, with reduced neuronal activity in spinal
300 sensorimotor circuits as a secondary change (58, 59). Increasing proprioceptive input to the
301 spinal cord may compensate for motor impairments in patients with SMA (60). In the present
302 study, we have shown the feasibility of selective and reversible induction and suppression of
303 large-diameter primary sensory afferent fiber activity using optogenetics. This novel
304 technique has a significant potential for advancing clinical research works on and therapeutic
305 approaches to conditioning spinal sensorimotor circuits, thereby offering new possibilities of
306 targeted interventions against CNS damage caused by stroke and neurodegenerative
307 disorders.
308

309 **Methods**

310 *Ethical approval*

311 All surgery was performed according to the institutional guidelines for animal experiments

312 and the National Institutes of Health Guide for the Care and Use of Laboratory Animals. All
313 experiments were approved by the experimental animal committee of the National Institute of
314 Neuroscience (approval number 2022020).
315
316 *Experimental animals*
317 Seventeen male Slc:Wistar rats (4 weeks old, 70–90 g) obtained from Japan SLC, Inc.
318 (Shizuoka, Japan) were used. All animals were housed under a normal light/dark cycle (12
319 h:12 h), with the light on from 08:00 h until 20:00 h, in a temperature-controlled environment
320 with food and water available ad libitum.
321
322 *Production of viral vectors*
323 AAV9-hSyn-ChR2(H134R)/EYFP (2.5×10^{13} genome copies/mL) (19) and AAV9-CMV-
324 eNpHR3.0/EYFP (1.8×10^{13} genome copies/mL) were produced using the helper-free triple
325 transfection procedure and purified by cesium chloride gradient. Viral titer was determined
326 by quantitative PCR using Taq-Man technology (Life Technologies, Gaithersburg, MD,
327 USA). Vector purity was assessed by 4–12% sodium dodecyl sulfate–polyacrylamide gel
328 electrophoresis and fluorescent staining (Oriole, Bio-Rad, Hercules, CA, USA). A transfer
329 plasmid (pAAV-CMV-eNpHR3.0-EYFP-WPRE) was constructed by inserting the
330 eNpHR3.0-EYFP fragment with a Woodchuck Hepatitis virus (WHV) posttranscriptional

331 regulatory element (WPRE) sequence into an AAV backbone plasmid (pAAV-CMV,

332 Stratagene, La Jolla, CA, USA).

333

334 *Vector injections*

335 ChR2 (*n* = 7) or eNpHR3.0 (*n* = 10) were transduced into DRG neurons by retrograde

336 transport following a sciatic nerve AAV injection (Fig. 1A). The protocol for AAV injection

337 was based on previous studies (19, 30). Briefly, animals were anesthetized by intraperitoneal

338 injection of medetomidine/midazolam/butorphanol anesthesia (0.2, 2.0, and 2.5 mg/kg,

339 respectively). Adequate depth of anesthesia was monitored frequently by monitoring pupil

340 size and flexion reflex to the paw pinch. After anesthesia, the animals were fixed in a prone

341 position, and an incision was made in the left gluteal muscle. The sciatic nerve was identified

342 below the biceps femoris muscle and isolated approximately 20 mm from the surrounding

343 tissue. A 31-gauge needle tube was inserted 10 mm into the isolated nerve. The needle tube

344 was connected by polyethylene tubing (JT- 10, EICOM, Kyoto, Japan) to a Hamilton syringe

345 (1702RN, GL Science, Tokyo, Japan) that was mounted into a microinjection pump

346 (LEGATO 180, KD Scientific, Holliston, MA, USA). The tubing, syringe, and needle tube

347 were filled with an electrically insulating stable fluorocarbon-based fluid (Fluorinert, 3M, St

348 Paul, MN, USA). Then 1% Fast Green (0.6 μL) was added to the viral vector solution to

349 visualize the injected solution. After insertion, the needle tube was left in place for 5 minutes

350 to allow sealing of the tissue around the needle tip. After, 3 μL of viral vector solution was
351 injected at a rate of 0.6 μL/min. The needle tube was removed at 10 minutes after the end of
352 the injection to ensure absorption of the solution. Two separate injections were performed
353 into the common peroneal and tibial branches of the sciatic nerve to ensure that the nerve was
354 filled uniformly (in total, 6 μL of viral vector solution was injected). Finally, the wound was
355 closed with a non-absorbable suture, and the animals were allowed to recover at 37°C.
356
357 *Acute electrophysiological experiments*
358 To test whether ChR2 and eNpHR3.0 could be used to recruit and inhibit activities of large-
359 diameter somatosensory afferents *in vivo*, an acute electrophysiological experiment was
360 performed 4–8 weeks after AAV injection. First, animals were anesthetized by intraperitoneal
361 injection of medetomidine/midazolam/butorphanol anesthesia (0.2, 2.0, and 2.5 mg/kg,
362 respectively). After a tracheotomy, anesthesia was maintained by inhalation of 0.5–1.0%
363 isoflurane throughout surgery. Electrocardiogram, oxygen saturation levels, and rectal
364 temperature were monitored and maintained within a physiological range.
365 To expose the lumbar spinal cord, a laminectomy was performed from the 1st
366 lumbar to the 1st sacral vertebrae. Then, the upper thoracic spine as well as the base of the
367 tail were immobilized using clamps. The dura was opened with a sharp needle, and the 4th
368 and 5th lumbar dorsal roots were separated from the other roots. For electrical and optical

369 stimulation, the left sciatic nerve was exposed and isolated from the surrounding tissue. The
370 skin and muscle around the exposed roots and nerves were raised and tied to form a pool,
371 which was filled with mineral oil to protect the exposed roots and nerves from drying out.
372 After surgery, anesthesia was maintained by thiopental sodium (10 mg/kg), and rocuronium
373 bromide (10 mg/kg) was administered intravenously to achieve neuromuscular blockade.
374 To apply electrical stimulation, a bipolar cuff electrode was mounted on the
375 isolated sciatic nerve. Stimulus current was generated using an isolator (SS 102L, Nihon
376 Kohden, Tokyo, Japan) coupled to an electrical stimulator (SEN7203, Nihon Kohden) with
377 various stimulus intensities (1–10-times threshold) at a fixed pulse width (100 μs). A
378 multimode optical fiber (960 μm in diameter, 0.63 numerical aperture; Doric Lenses, Quebec,
379 Canada) connected to a light source (LISER_LED470, Doric Lenses) was placed 10 mm
380 proximal to the cuff electrode to ensure the stimulus site was not directly irradiated (Fig. 1E).
381 To record stimulus-evoked volleys, a bipolar hook electrode was mounted on the
382 isolated dorsal root at 15–25 mm proximal to DRG. Recorded potentials were amplified (×
383 1000) and band-pass filtered (15–10 kHz) using an amplifier (MEG-6108M, Nihon Kohden),
384 and digitized at 50 kHz using an analog/digital converter (Digidata 1550, Molecular Devices,
385 LLC, San Jose, CA, USA). The average of 20 responses, consisting of a 10 ms pre-stimulus
386 baseline period followed by a 100 ms post-stimulus period, was obtained. Then, the peak-to-
387 peak amplitude and latency between onset of the stimulus and beginning of the response were

388 calculated. The beginning of the response was defined as a time that exceeded the value of
389 the mean ± 3× standard deviations of the background signal recorded 10 ms before the
390 stimulation.

391 To confirm the effect of optical facilitation, optical stimulation of blue light at 470
392 nm was applied to the sciatic nerve. The stimulation was applied 20-times with a fixed
393 stimulus duration (1 ms) at an interval of 0.5 s (2 Hz). To test whether the effect of optical
394 stimulation was caused by activation of ChR2, irradiation at a different wavelength (593 nm,
395 1 ms duration) was also performed. To characterize the response properties of optical
396 facilitation, intensity–response characteristics of the irradiated light power were examined by
397 changing the intensity of light power (11.4–127.2 mW) at a fixed stimulus duration (1 ms).
398 To test whether optical stimulation activated large-diameter afferents selectively, intensity–
399 response characteristics with longer light pulse duration (10 ms) were further examined
400 because longer and stronger optical stimulation can recruit high-threshold non-target fibers
401 (19). The light power was measured at the tip of the optical fiber using a power meter
402 (PM100D, Thorlabs, Newton, New Jersey, USA). To facilitate comparison across animals,
403 volley amplitudes were normalized to the maximum amplitude of electrically evoked volleys
404 (10-times threshold intensity).

405 To confirm the effect of optical inhibition, three experimental sessions were
406 performed: a baseline session (“Baseline”, light-off condition), a session during irradiation of

407 yellow light at 593 nm (“Light”, light-on condition), and a session immediately following
408 light deactivation (“Recovery”, light-off condition). Each session consisted of 20 electrical
409 stimuli at an interval of 0.5 s (2 Hz) and proceeded consequently without a break. Yellow
410 light was continuously irradiated for 10 s in only the “Light” session. To facilitate
411 comparison across animals, volley amplitudes in the “Light” and “Recovery” sessions were
412 normalized against the averaged amplitude in the preceding “Baseline” session. Considering
413 reported side effects of light irradiation, such as heating (14, 61−63) and light-off rebound
414 effects (64), the reversibility of light irradiation was confirmed by comparing “Baseline” and
415 “Recovery” sessions. Because prolonged light irradiation can decrease the efficacy of
416 inhibition over time (63, 65, 66), the temporal stationarity of optical inhibition was confirmed
417 by calculating the correlation between the elapsed time of light irradiation for each stimulus
418 and the peak-to-peak amplitude of each volley in the “Light” session.

419 To characterize the response properties of optical inhibition, three sessions were
420 repeated under various conditions. First, intensity–response characteristics of irradiated light
421 power were examined by changing the light power intensity (8.7–107.3 mW) at a fixed
422 electrical stimulation (1.5-times threshold intensity). Then, intensity–response characteristics
423 of electrical stimulation were examined by changing the intensity of electrical stimulation (1–
424 5-times threshold) at a fixed light power (107.3 mW). The percentage of amplitude inhibition
425 was calculated as the difference in normalized amplitude between “Baseline” and “Light”

426 sessions. The latency difference was also calculated as the difference in latency between
427 "Baseline" and "Light" sessions and compared in each condition.
428 At the end of the experiments, small electrolytic lesions were made in the dorsal
429 root and sciatic nerve using a 40 μA direct current stimulation of the recording and
430 stimulating bipolar hook electrodes for 40 s. Then, the animals were deeply anesthetized by
431 intravenous injection of thiopental sodium (20 mg/kg) and perfused transcardially with
432 phosphate-buffered saline (pH 7.4), followed by 300 mL of 10% neutral buffered
433 formaldehyde. After perfusion, the lumbar region of the spinal cord together with the DRG
434 and sciatic nerve were removed.
435
436 *Histological quantification*
437 To check expression of ChR2 and eNpHR3.0, the fluorescent signal intensity of YFP was
438 examined. Fluorescent images of entire DRG neurons were acquired using an inverted
439 microscope (BZ-X710, Keyence, Osaka, Japan) using fixed detector gain values without
440 sectioning. To calculate the fluorescent intensity, the images were converted to grayscale, and
441 then mean gray values within the region of interest were determined manually.
442
443 *Statistical analyses*
444 The Wilcoxon signed-rank test was performed for all two group comparisons. For group

analysis, Friedman's test was performed with light power or recording sessions ("Baseline", "Light", and "Recovery" sessions) as a within-subject factor. One-way ANOVA was performed with three recording sessions only for single animal analysis in the optical inhibition experiment. Post hoc analyses were performed using Tukey's or Dunn's tests for multiple comparisons. When testing intensity–response characteristics of electrical stimulation in the optical inhibition experiment, one-tailed Wilcoxon signed-rank test with Holm–Bonferroni correction was performed to compare the percentage of amplitude inhibition in each stimulus intensity to the hypothetical value (0% inhibition). For all correlation analyses, Pearson's correlation coefficient was calculated. The level of significance was set at $\alpha = 0.05$. All electrophysiological data were analyzed using MATLAB 2021b (MathWorks, Natick, MA, USA), all fluorescent images were analyzed using OpenCV 4.6.0 with python 3.8, and all statistical tests were performed using Prism 10 (GraphPad Software, San Diego, CA, USA).

Acknowledgments:

We thank Dr. Hidemasa Furue for their helpful comments. Dr. Wupuer Sidikejiang, Dr. Shinji Kubota, and Ms. Moeko Kudo for their technical assistance. This work was supported by a Grant-in-Aid from the Japan Society for the Promotion of Science (JSPS) (grant numbers JP19H05724, JP19H01092, JP26120003, and JP 23H05488 [to K.S.], JP22H04922 [to K. I.],

464 and JP21K17633 [to A.K.]), and research grants from the Japan Agency for Medical
465 Research and Development (AMED) (grant numbers JP21dm0207092, JP21dm0207066, and
466 JP19ek0109216 [to K.S.], and JP21dm0207077 [to K.S. and M.T.]).

467

468 **Author contributions:**

469 A.K. and K.S. designed the study. K.I. and M.T. developed the viral vectors. A.K. performed
470 the surgery and electrophysiological experiments. A.K. analyzed the data. A.K. and K.S.
471 wrote a draft of the manuscript. All authors approved the final version of the manuscript.

472

473 **Declaration of interests:** The authors declare they have no competing interests.

474

References

1. Woolf, C.J., and Salter, M.W. (2000). Neuronal plasticity: increasing the gain in pain. *Science* **288**, 1765–1769.
2. Navarro, X., Vivó, M., and Valero-Cabré, A. (2007). Neural plasticity after peripheral nerve injury and regeneration. *Prog. Neurobiol*. **82**, 163–201.
3. Navarro, X., Krueger, T.B., Lago, N., Micera, S., Stieglitz, T., and Dario, P. (2005). A critical review of interfaces with the peripheral nervous system for the control of neuroprostheses and hybrid bionic systems. *J. Peripher. Nerv. Syst.* **10**, 229–258.
4. Goins, W.F., Cohen, J.B., and Glorioso, J.C. (2012). Gene therapy for the treatment of chronic peripheral nervous system pain. *Neurobiol. Dis.* **48**, 255–270.
5. Chang, R.B. (2019). Optogenetic control of the peripheral nervous system. *Cold Spring Harb. Perspect Med.* **9**, a034397.
6. Graham, R.D., Sankarasubramanian, V., and Lempka, S.F. (2022). Dorsal Root Ganglion Stimulation for Chronic Pain: Hypothesized Mechanisms of Action. *J. Pain* **23**, 196–211.
7. Daou, I., Beaudry, H., Ase, A.R., Wieskopf, J.S., Ribeiro-da-silva, A., Mogil, J.S., and Séguéla, P. (2016). Optogenetic Silencing of $Na_V1.8$-Positive Afferents. *eNeuro* **3**, ENEURO.0140-15.2016.
8. Montgomery, K.L., Iyer, S.M., Christensen, A.J., Deisseroth, K. and Delp, S. L. (2016). Beyond the brain: Optogenetic control in the spinal cord and peripheral nervous system. *Sci. Trans. Med.* **8**, 337rv5.
9. Boyden, E.S., Zhang, F., Bamberg, E., Nagel, G., and Deisseroth, K. (2005). Millisecond-timescale, genetically targeted optical control of neural activity. *Nat. Neurosci.* **8**, 1263–1268.
10. Nagel, G., Brauner, M., Liewald, J.F., Adeishvili, N., and Bamberg, E. (2005). Light activation of Channelrhodopsin-2 in excitable cells of *caenorhabditis elegans* triggers rapid behavioral responses. *Curr. Biol.* **15**, 2279–2284.

11. Zhang, F., Wang, L.P., Brauner, M., Liewald, J.F., Kay, K., Watzke, N., Wood, P.G. Bamberg, E., Nagel, G., Gottschalk, A. et al. (2007). Multimodal fast optical interrogation of neural circuitry. *Nature* **446**, 633–639.
12. Deisseroth, K. (2011). Optogenetics. *Nat. Methods* **8**, 26–29.
13. Deisseroth, K. (2015). Optogenetics: 10 years of microbial opsins in neuroscience. *Nat. Neurosci.* **18**, 1213–1225.
14. Yizhar, O., Fenno, L. E., Davidson, T. J., Mogri, M., and Deisseroth, K. (2011). Optogenetics in Neural Systems. *Neuron* **71**, 9–34.
15. Piatkevich, K.D., and Boyden, E.S. (2023). Optogenetic control of neural activity: The biophysics of microbial rhodopsins in neuroscience. *Q. Rev. Biophys.* **57**, e1.
16. Daou, I., Tuttle, A.H., Longo, G., Wieskopf, J.S., Bonin, R.P., Ase, A.R., Wood, J.N., de Koninck, Y., Ribeiro-da-Silva, A., Mogil, J.S. et al. (2013). Remote optogenetic activation and sensitization of pain pathways in freely moving mice. *J. Neurosci.* **33**, 18631–18640
17. Boada, M.D., Martin, T.J., Peters, C.M., Hayashida, K., Harris, M.H., Houle, T.T., Boyden, E.S., Eisenach, J.C., and Riri, D.G. (2014). Fast-conducting mechanoreceptors contribute to withdrawal behavior in normal and nerve injured rats. *Pain* **155**, 2646–2655.
18. Iyer, S.M., Montgomery, K.L., Towne, C., Lee, S.Y., Ramakrishnan, C., Deisseroth, K., and Delp, S.L. (2014). Virally mediated optogenetic excitation and inhibition of pain in freely moving nontransgenic mice. *Nat. Biotechnol.* **32**, 274–278.
19. Kubota, S., Sidikejiang, W., Kudo, M., Inoue, K., Umeda, T., Takada, M., and Seki, K. (2019). Optogenetic recruitment of spinal reflex pathways from large-diameter primary afferents in non-transgenic rats transduced with AAV9/Channelrhodopsin 2. *J. Physiol.* **597**, 5025–5040.
20. Fischer, G., Kostic, S., Nakai, H., Park, F., Sapunar, D., Yu, H., and Hogan, Q. (2011). Direct injection into the dorsal root ganglion: Technical, behavioral, and histological observations. *J. Neurosci. Methods* **199**, 43–55.

21. Yang, O.J., Robilotto, G.L., Alom, F., Alemán, K., Devulapally, K., Morris, A., and Mickle A.D. (2023). Evaluating the transduction efficiency of systemically delivered AAV vectors in the rat nervous system. *Front. Neurosci.* **17**, 1001007.
22. Llewellyn, M.E., Thompson, K.R., Deisseroth, K., and Delp, S.L. (2010). Orderly recruitment of motor units under optical control in vivo. *Nat. Med.* **16**, 1161–1165.
23. Liske, H., Towne, C., Anikeeva, P., Zhao, S., Feng, G., Deisseroth, K., and Delp, S.L. (2013). Optical inhibition of motor nerve and muscle activity in vivo. *Muscle and Nerve* **47**, 916–921.
24. Maimon, B.E., Sparks, K., Srinivasan, S., Zorzos, A.N., and Herr, H.M. (2018). Spectrally distinct channelrhodopsins for two-colour optogenetic peripheral nerve stimulation. *Nat. Biomed. Eng*. **2**, 485–496.
25. Williams, J.J., Watson, A.M., Vazquez, A.L., and Schwartz, A.B. (2019). Viral-mediated optogenetic stimulation of peripheral motor nerves in non-human primates. *Front. Genet.* **13**, 759.
26. Stewart, J.D. (2003). Peripheral nerve fascicles: Anatomy and clinical relevance. *Muscle and Nerve* **28**, 525–541.
27. Hochman, S. (2007). Spinal cord. *Curr. Biol.* **17**, R950-5.
28. Abraira, V.E., and Ginty, D.D. (2013). The sensory neurons of touch. *Neuron* **79**, 618–639.
29. Gatto, G., Smith, K.M., Ross, S.E., and Goulding, M. (2019). Neuronal diversity in the somatosensory system: bridging the gap between cell type and function. *Curr. Opin. Neurobiol*. **56**, 167–174.
30. Kudo, M., Wupuer, S., Fujiwara, M., Saito, Y., Kubota, S., Inoue, K., Takada, M., and Seki K. (2021). Specific gene expression in unmyelinated dorsal root ganglion neurons in nonhuman primates by intra-nerve injection of adeno-associated virus 6 vector. *Mol. Ther. Methods Clin. Dev.* **23**, 11–22.
31. Harper, A.A., and Lawson, S.N. (1985). Conduction velocity is related to morphological cell type in rat dorsal root ganglion neurones. *J. Physiol*. **359**, 31-46.
32. Brock, L.G., Eccles, J.C., and Rall, W. (1951). Experimental investigations on the

afferent fibres in muscle nerves. *Proc. R. Soc. Lond. B Biol. Sci.* **138**, 453–475.

33. Bradley, K., and Eccles, J.C. (1953). Analysis of the fast afferent impulses from thigh muscles. *J. Physiol.* **122**, 462–473.
34. Arlow, R.L., Foutz, T.J., and McIntyre, C.C. (2013). Theoretical principles underlying optical stimulation of myelinated axons expressing channelrhodopsin-2. *Neuroscience* **248**, 541–551.
35. McNeal, D.R. (1976). Analysis of a model for excitation of myelinated nerve. *IEEE Trans. Biomed. Eng.* **23**, 329–337.
36. Lertmanorat, Z., and Durand, D.M. (2004). Extracellular voltage profile for reversing the recruitment order of peripheral nerve stimulation: A simulation study. *J Neural. Eng.* **1**, 202–211.
37. Erlanger, J., and Gasser, H.S. (1937). Electrical Signs of Nervous Activity. *University Pennsylvania Press*, Philadelphia.
38. Lloyd, D.P.C. (1946). Integrative pattern of excitation and inhibition in two-neuron reflex arcs. *J. Neurophysiol.* **9**, 439–444.
39. Boyd, I.A., and Kalu. K.U. (1979). Scaling factor relating conduction velocity and diameter for myelinated afferent nerve fibres in the cat hind limb. *J. Physiol.* **289**, 277–297.
40. Iyer, S. M., Vesuna, S., Ramakrishnan, C., Huynh, K., Young, S., Berndt, A., Lee, S. Y., Gorini, C.J., Deisseroth, K., and Delp, S.L. (2016). Optogenetic and chemogenetic strategies for sustained inhibition of pain. *Sci. Rep.* **6,** 30570.
41. Li, B., Yang, X.Y., Qian, F.P., Tang, M., Ma, C., and Chiang, L.Y. (2015). A novel analgesic approach to optogenetically and specifically inhibit pain transmission using TRPV1 promoter. *Brain Res.* **1609**, 12–20.
42. Mayer, P., Sivakumar, N., Pritz, M., Varga, M., Mehmann, A., Lee, S., Salvatore, A. Magno, M., Pharr, M., Johannssen, H.C. et al. (2019). Flexible and lightweight devices for wireless multi-color optogenetic experiments controllable via commercial cell phones. *Front. Neurosci.* **13**, 819.
43. Schuster, D.J., Dykstra, J.A., Riedl, M.S., Kitto, K.F., Belur, L.R., McIvor, R.S., Elde,

587 R.P., Fairbanks, C.A., and Vulchanova, L. (2014). Biodistribution of adeno-associated
588 virus serotype 9 (AAV9) vector after intrathecal and intravenous delivery in mouse.
589 *Front. Neuroanat.* **8**, 42.
590 44. Harding, E.K., Fung, S.W., and Bonin R.P. (2020). Insights Into Spinal Dorsal Horn
591 Circuit Function and Dysfunction Using Optical Approaches. *Front. Neural Circuits* **14**,
592 31.
593 45. Park, S.I., Brenner, D.S., Shin, G., Morgan, C.D., Copits, B.A., Chung, H.U., Pullen,
594 M.Y., Noh, K.N., Davidson, S., Oh, S.J. et al. (2015). Soft, stretchable, fully implantable
595 miniaturized optoelectronic systems for wireless optogenetics. *Nat. Biotechnol.* **33**,
596 1280–1286.
597 46. Mondello, S.E., Sunshine, M.D., Fischedick, A.E., Dreyer, S.J., Horwitz, X.G.D.,
598 Anikeeva, P., Horner, P.J., and Moritz, C.T. (2018). Optogenetic surface stimulation of
599 the rat cervical spinal cord. *J. Neurophysiol.* **120**, 795–811.
600 47. Kent, A.R., Min, X., Hogan, Q.H., and Kramer, J.M. (2018). Mechanisms of Dorsal Root
601 Ganglion Stimulation in Pain Suppression: A Computational Modeling Analysis.
602 *Neuromodulation* **21**, 234–246.
603 48. Graham, R.D., Bruns, T.M., Duan, B., and Lempka, S.F. (2019). Dorsal root ganglion
604 stimulation for chronic pain modulates Aβ-fiber activity but not C-fiber activity: A
605 computational modeling study. *Clin. Neurophysiol.* **130**, 941–951.
606 49. Du, H., Hao, S., Gigout, D., Huang, Y., Yang, L., Li, C., Wang, D., Sundt, D.B. Jaffe, H.
607 Zhang, N. et al. (2014). Control of somatic membrane potential in nociceptive neurons
608 and its implications for peripheral nociceptive transmission. *Pain* **155**, 2306–2322.
609 50. Sundt, D., Gamper, N., and Jaffe, D.B. (2015). Spike propagation through the dorsal root
610 ganglia in an unmyelinated sensory neuron: A modeling study. *J. Neurophysiol.* **114**,
611 3140–3153.
612 51. Sperry, Z.J., Graham, R.D., Peck-Dimit, N., Lempka, S.F., and Bruns, T.M. (2020).
613 Spatial models of cell distribution in human lumbar dorsal root ganglia. *J. Comp. Neurol.*
614 **528**, 1644–1659.
615 52. Towne, C., Montgomery, K.L., Iyer, S.M., Deisseroth, K., and Delp, S.L. (2013).

Optogenetic Control of Targeted Peripheral Axons in Freely Moving Animals. *PLoS ONE* **8**, e72691.

53. Michoud, F., Sottas, L., Browne, L.E., Asboth, L., Latremoliere, A., Sakuma, M., Courtine, G., Woolf, C.J., and Lacour, S.P. (2018). Optical cuff for optogenetic control of the peripheral nervous system. *J. Neural. Eng.* **15**, 015002.
54. Song, K.I., Park, S.E., Lee, S., Kim, H., Lee, S.H., and Youn, I. (2018). Compact Optical Nerve Cuff Electrode for Simultaneous Neural Activity Monitoring and Optogenetic Stimulation of Peripheral Nerves. *Sci. Rep.* **8**, 15630.
55. Maimon, B.E., Zorzos, A.N., Bendell, R., Harding, A., Fahmi, M., Srinivasan, S. Calvaresi, P. and Herr H.M. (2017). Transdermal optogenetic peripheral nerve stimulation. *J. Neural. Eng.* **14**, 34002.
56. Burke, D., Wissel, J., and Donnan, G.A. (2013). Pathophysiology of spasticity in stroke. *Neurology* **80**, S20–26.
57. Li, S., and Francisco, G.E. (2015). New insights into the pathophysiology of post-stroke spasticity. *Front. Hum. Neurosci.* **9**, 192.
58. Mentis, G.Z., Blivis, D., Liu, W., Drobac, E., Crowder, M.E., Kong, L., Alvarez, F. J., Sumner, C.J., and O'Donovan, M.J. (2011). Early functional impairment of sensory-motor connectivity in a mouse model of spinal muscular atrophy. *Neuron* **69**, 453–467.
59. Fletcher, E.V., Simon, C.M., Pagiazitis, J.G., Chalif, J.I., Vukojicic, A., Drobac, E., Wang, X., and Mentis, G.Z. (2017). Reduced sensory synaptic excitation impairs motor neuron function via Kv2.1 in spinal muscular atrophy. *Nat. Neurosci.* **20**, 905–916.
60. Simon, C.M., Blanco-Redondo, B., Buettner, J.M., Pagiazitis, J.G., Fletcher, E.V., Sime Longang, J.K., and Mentis, G.Z. (2021). Chronic Pharmacological Increase of Neuronal Activity Improves Sensory-Motor Dysfunction in Spinal Muscular Atrophy Mice. *J. Neurosci.* **41**, 376–389.
61. Stujenske, J.M., Spellman, T., and Gordon, J.A. (2015). Modeling the Spatiotemporal Dynamics of Light and Heat Propagation for In Vivo Optogenetics. *Cell Rep.* **12**, 525–534.

62. Arias-Gil, G., Ohl, F.W., Takagaki, K., and Lippert, M.T. (2016). Measurement, modeling, and prediction of temperature rise due to optogenetic brain stimulation. *Neurophotonics* **3**, 045007.
63. Wiegert, J.S., Mahn, M., Prigge, M., Printz, Y., and Yizhar, O. (2017). Silencing Neurons: Tools, Applications, and Experimental Constraints. *Neuron* **95**, 504–529.
64. Bansal, H., Gupta, N., and Roy, S. (2020). Comparison of low-power, high-frequency and temporally precise optogenetic inhibition of spiking in NpHR, eNpHR3.0 and Jaws-expressing neurons. *Biomed. Phys. Eng. Express* **6,** 045011.
65. Mattis, J., Tye, K.M., Ferenczi, E.A., Ramakrishnan, C., O'Shea, D.J., Prakash, R., Gunaydin, L.A., Hyun, M., Fenno, L.E., Gradinaru, V. et al. (2011). Principles for applying optogenetic tools derived from direct comparative analysis of microbial opsins. *Nat. Methods* **9**, 159–172.
66. Zhang, C., Yang, S., Flossmann, T., Gao, S., Witte, O.W., Nagel, G., Holthoff, K., and Kirmse, K.(2019). Optimized photo-stimulation of halorhodopsin for long-term neuronal inhibition. *BMC Biol.* **17**, 95.

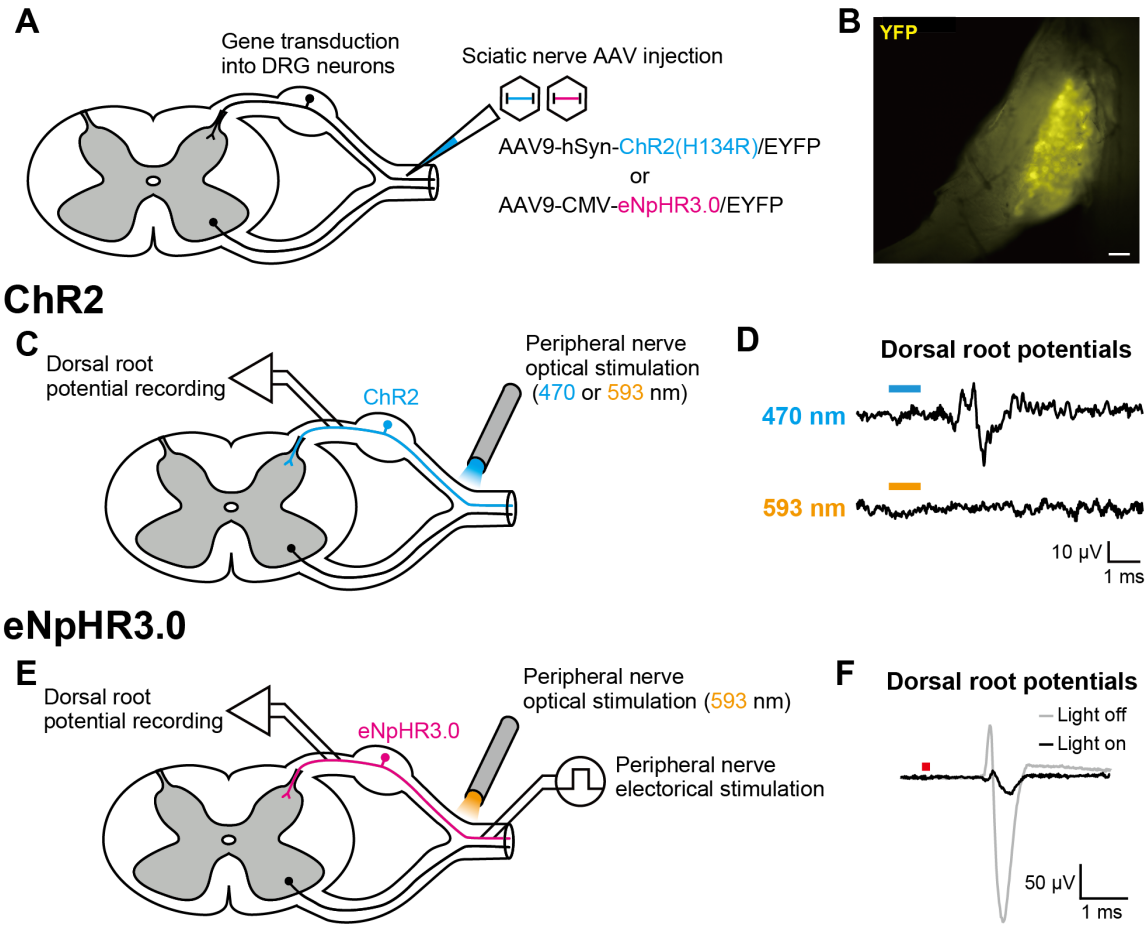

Figure 1. Optogenetic manipulation of sensory afferent activity by adeno-associated virus serotype 9 (AAV9)-mediated gene transduction into dorsal root ganglion (DRG) neurons and optical stimulation of nerve fibers. (A) Schema of AAV injection. Retrograde transport via sciatic nerve injection enabled gene transduction into DRG neurons. (B) Expression of YFP in the 5th lumbar DRG neurons. Scale bar: 200 μm. (C, D) Results on channelrhodopsin (ChR2) transduction. (C) Schema of the acute *in vivo* electrophysiological experiment. (D) Examples of dorsal root potentials evoked by light stimulation with different wavelengths. Waveforms represent the stimulus-triggered averaging of 20 responses. The bar above each waveform indicates the timing of light irradiation. (E, F) Results on

670 halorhodopsin (eNpHR3.0) transduction. **(**E) Schema of the acute *in vivo* electrophysiological

671 experiment. (F) Examples of electrically evoked volleys with (black line) and without (gray

672 line) light irradiation. Waveforms represent the stimulus-triggered averaging of 20 responses.

673 The red square above the waveforms indicates the timing of electrical stimulation.

674

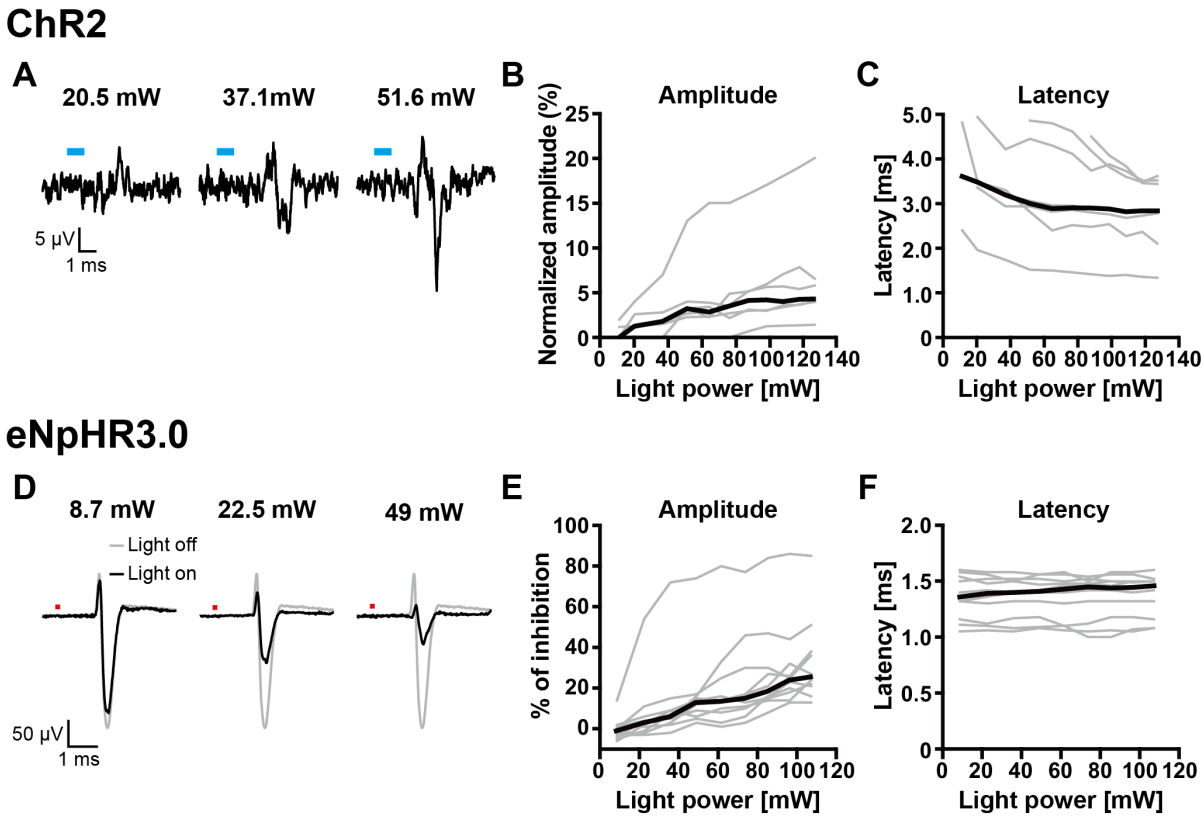

Figure 2. Effect of light power on optogenetic manipulation. (A−C) Results on channelrhodopsin (ChR2) transduction. (A) Examples of recruited volleys using different irradiated light powers. Waveforms represent the stimulus-triggered averaging of 20 responses. Blue bars above each waveform indicates the timing of light irradiation. (B, C) Changes in the amplitude and latency of recruited volleys as a function of light power. Each gray line represents one animal (n = 7), and thick black lines represent the median value of all animals. (D−F) Results on halorhodopsin (eNpHR3.0) transduction. (D) Examples of electrically evoked volleys using different irradiated light powers. Waveforms represent the stimulus-triggered averaging of 20 responses. Black lines indicate electrically evoked volleys with light irradiation and gray lines indicate volleys without irradiation. Red squares above

686 each waveform indicates the timing of electrical stimulation. (E, F) Changes in the

687 percentage of amplitude inhibition and latency of electrically evoked volleys as a function of

688 light power. Each gray line represents one animal (n = 10), and thick black lines represent the

689 median value of all animals.

690

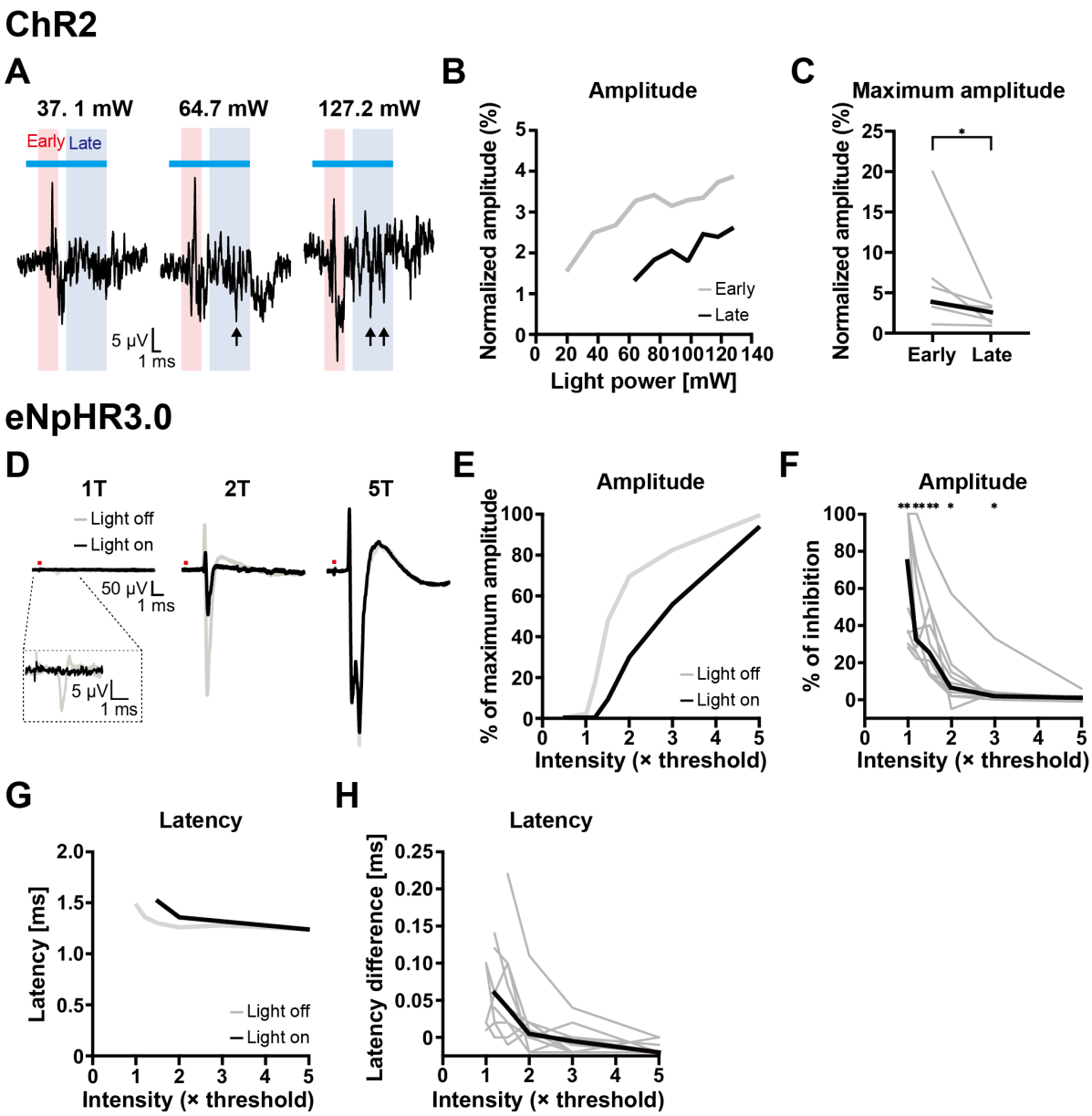

Figure 3. Large-diameter afferent preference. (A–C) Results of channelrhodopsin (ChR2) transduction. (A) Examples of recruited volleys using long light pulse durations. Waveforms represent the stimulus-triggered averaging of 20 responses. Red shading indicates the range of early-onset volleys (1.5–4 ms after stimulus onset), and blue shading indicates the range of late-onset volleys (5–10 ms after stimulus onset). Blue bars above the waveforms indicate the timing of light irradiation. Black arrows indicate individual peaks of late-onset volleys. (B)

Changes in normalized amplitude of early- and late-onset volleys as a function of light power. The gray line indicates the early-onset component, and the black line indicates the late-onset component. Note that each line is plotted only at the light power at which the volley was observed. (C) Maximum normalized amplitude of early- and late-onset volleys evoked by long light pulse duration. Each gray line represents one animal ($n = 7$), and thick black lines represent the median value of all animals. *$p < 0.05$ (Wilcoxon signed-rank test). (D–H) Results of halorhodopsin (eNpHR3.0) transduction. (D) Examples of electrically evoked volleys using different intensities of electrical stimulation. Waveforms represent the stimulus-triggered averaging of 20 responses. Black lines indicate electrically evoked volleys using light irradiation and gray lines indicate volleys without irradiation. Red squares above each waveform indicates the timing of electrical stimulation. (E) Example of intensity–response curves of amplitudes with and without light irradiation from one animal. (F) Changes in the percentage of amplitude inhibition as a function of electrical stimulation intensity. Each gray line represents one animal ($n = 10$), and thick black lines represent the median value of all animals. *$p < 0.05$; **$p < 0.01$ (one-tailed Wilcoxon signed-rank test with Holm–Bonferroni correction compared to 0%). (G) Example of intensity–response curves of latency with and without light irradiation from one animal. (H) Difference in latency as a function of electrical stimulation intensity. Each gray line represents one animal ($n = 10$), and thick black lines represent the median value of all animals.

717

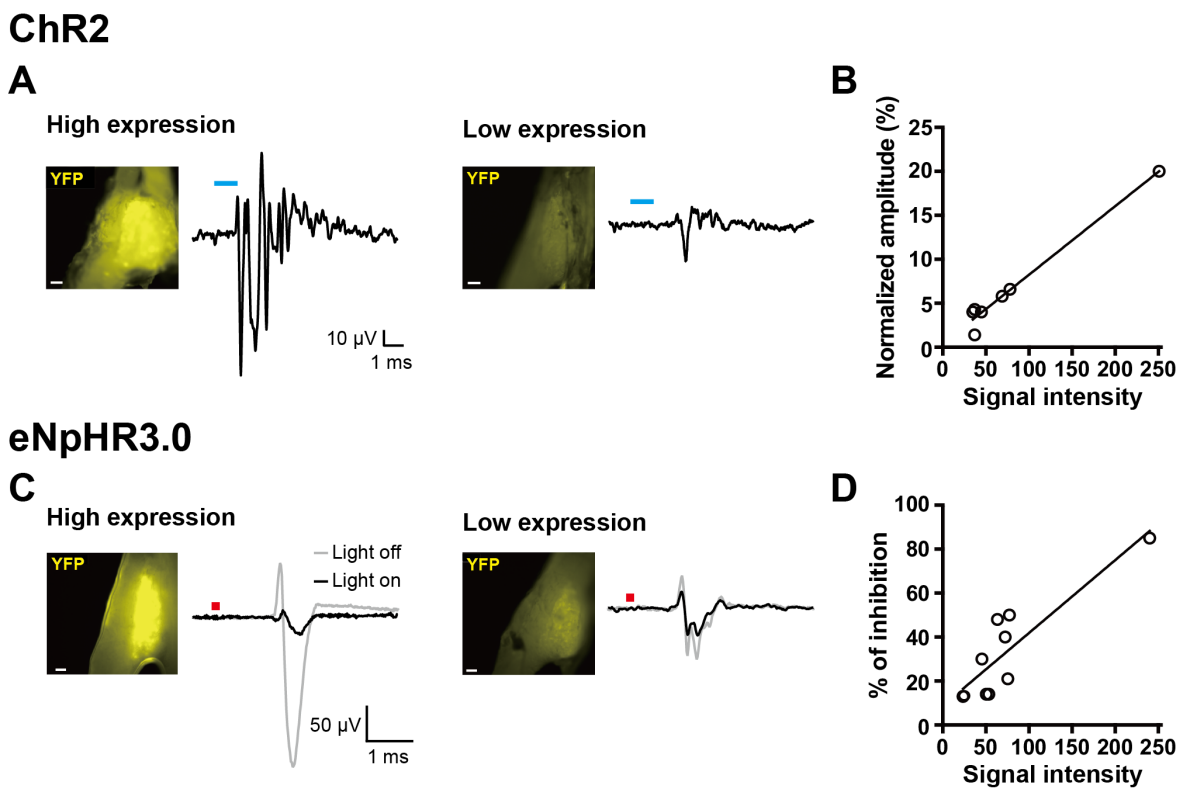

Figure 4. Correlation between optical efficacy and YFP intensity. (A, B) Results on channelrhodopsin (ChR2) transduction. (A) Examples of recruited volleys and YFP expression in dorsal root ganglion (DRG) neurons for two animals with different expression levels. Waveforms represent the stimulus-triggered averaging of 20 responses. Blue bars above each waveform indicates the timing of light irradiation. Scale bar: 200 μm. (B) Scatter plots and linear correlation between the normalized amplitude and YFP signal intensity of all animals (n = 7). (C, D) Results on halorhodopsin (eNpHR3.0) transduction. (C) Examples of electrically evoked volleys with (black line) and without (gray line) light irradiation and YFP expression in DRG neurons for two animals with different expression levels. Waveforms represent stimulus-triggered averaging of 20 responses. Red squares above the waveforms

729 indicate the timing of electrical stimulation. Scale bar: 200 μm. (D) Scatter plots and linear

730 correlation between the amplitude inhibition percentage and YFP signal intensity of all

731 animals (n = 10).

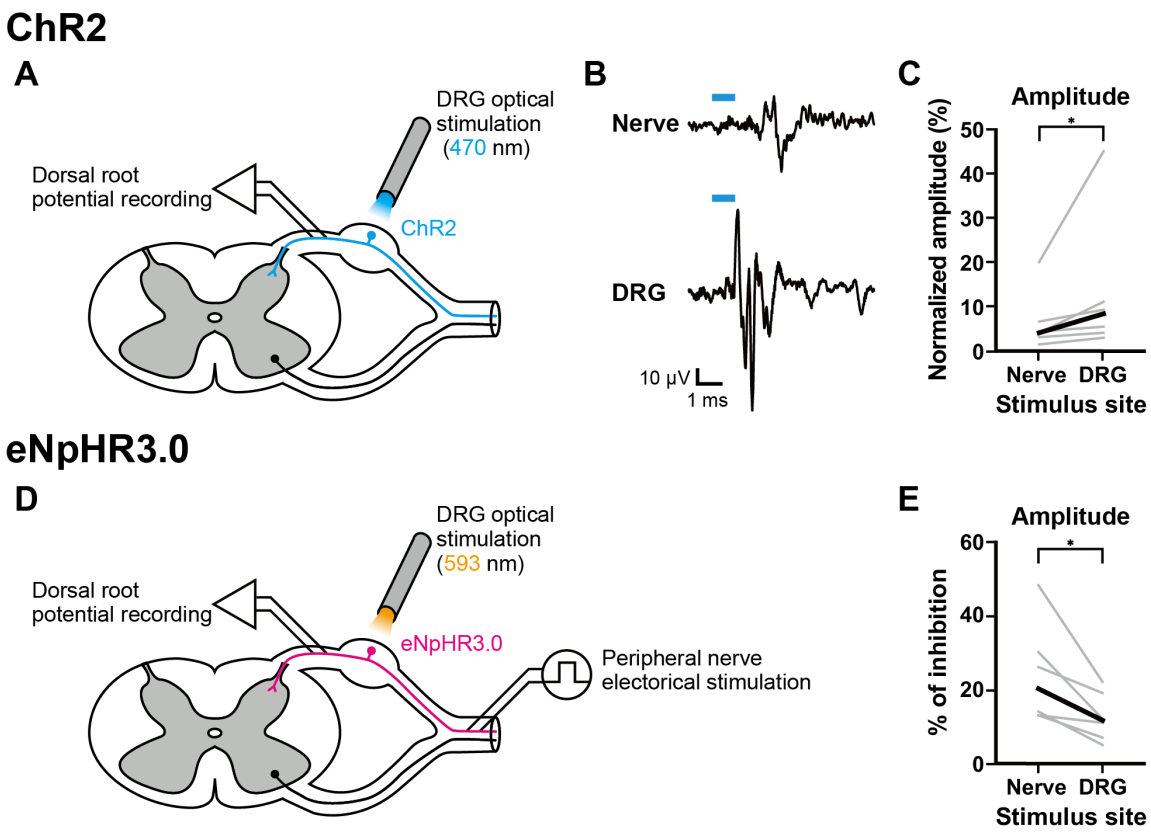

Figure 5. Sites and effects of optical stimulation. (A–C) Results on channelrhodopsin (ChR2) transduction. (A) Schema of the acute *in vivo* electrophysiological experiment. (B) Examples of recruited volleys by optical stimulation to the sciatic nerve and dorsal root ganglion (DRG). Waveforms represent the stimulus-triggered averaging of 20 responses. Blue bars above the waveforms indicate the timing of light irradiation. (C) The effect of the stimulus site on the amplitude. Each gray line represents one animal (n = 7), and thick black lines represent the median value of all animals. (D, E) Results on halorhodopsin (eNpHR3.0) transduction. (D) Schema of the acute *in vivo* electrophysiological experiment. (E) The effect of the stimulus site on the percentage of amplitude inhibition. Each gray line represents one animal (n = 6), and thick black lines represent the median value of all animals. *$p < 0.05$.

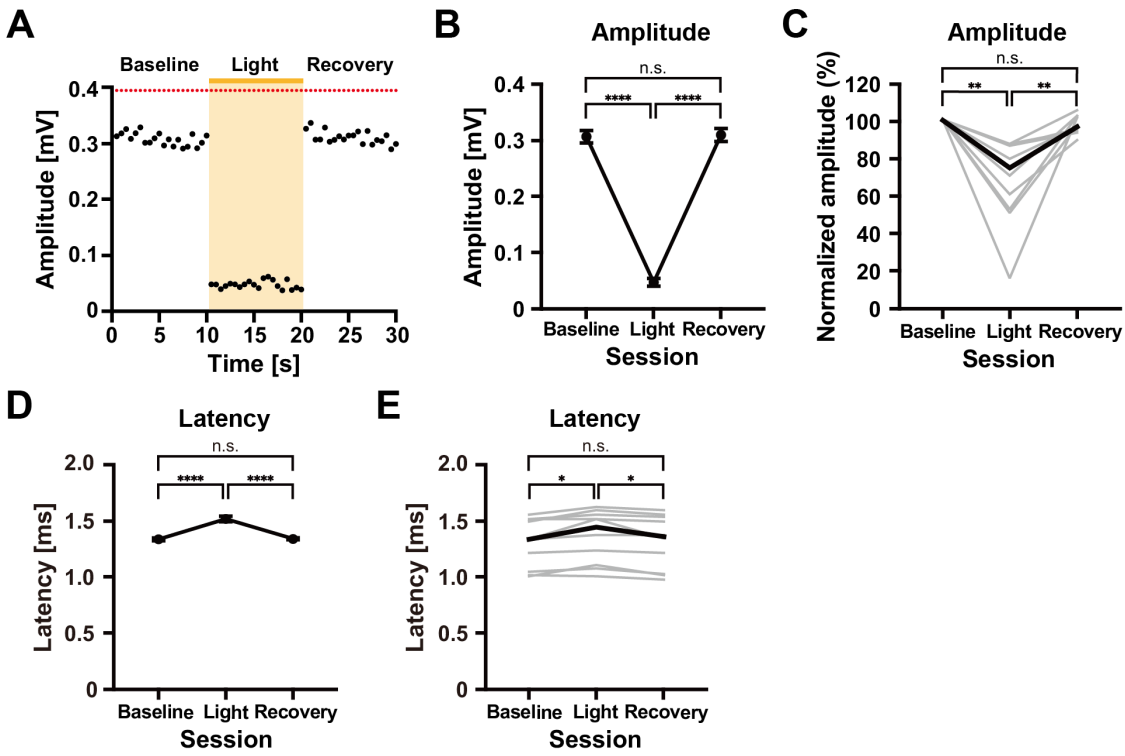

Figure S1. Characterization of optogenetic suppression. (A) Time course of peak-to-peak amplitudes of electrically evoked volleys. Red dots indicate the timing of electrical stimulation (2 Hz). The orange line and orange shaded area indicate the timing of light irradiation (10 s). There was no significant correlation between the elapsed time of light irradiation and the peak-to-peak amplitude in the "Light" session (r = -0.073, p = 0.76), indicating no time trend in this session. (B, C) Effect of optical inhibition on the amplitude from a representative animal (B) and for all animals (C). For representative animal, data are represented mean ± standard deviation. For all animals, amplitudes in the "Light" and "Recovery" sessions were normalized by the average amplitude in the preceding "Baseline" session. Each gray line represents one animal (n = 10), and thick black lines represent the median value of all animals. Significant differences were found between the "Baseline" and

755 the “Light” session in a representative animal (one-way analysis of variance [ANOVA], $F_{(2,57)}$

756 = 4365, $p < 0.0001$; Tukey’s post hoc test, $p < 0.0001$), and all animals (Friedman’s test,

757 $\chi^2_{(2,18)} = 15.2$, $p < 0.0001$, Dunn’s post hoc test, $p = 0.001$). No difference was seen between

758 the “Baseline” and the “Recovery” session ($p = 0.61$ in the representative animal and $p = 0.99$

759 in all animals), suggesting that light irradiation causes no side effects. (D, E) Effect of optical

760 inhibition on latency from a representative animal (D) and for all animals (E). For

761 representative animal, data are represented mean ± standard deviation. For all animals, each

762 gray line represents one animal ($n = 10$), and thick black lines represent the median value of

763 all animals. The onset latency of the volley in the “Light” session was significantly longer

764 than that in the “Baseline” session in a representative animal (one-way ANOVA, $F_{(2,57)}$ =

765 742.3, $p < 0.0001$; Tukey’s post hoc test, $p < 0.0001$), and all animals (Friedman’s test, $\chi^2_{(2,18)}$

766 = 10.6, $p = 0.002$, Dunn’s post hoc test, $p = 0.011$). No difference was found between the

767 “Baseline” and the “Recovery” session ($p = 0.79$ in the representative animal and $p = 0.99$ in

768 all animals), suggesting the reversible nature of latency inhibition. *$p < 0.05$; **$p < 0.01$;

769 ****$p < 0.0001$.

770